

Letter

# Assessing the Impact of Corona-Virus-19 on Nitrogen Dioxide Levels over Southern Ontario, Canada

Debora Griffin <sup>1,\*</sup>, Chris Anthony McLinden <sup>1,2</sup>, Jacinthe Racine <sup>3</sup>, Michael David Moran <sup>1</sup>, Vitali Fioletov <sup>1</sup>, Radenko Pavlovic <sup>3</sup>, Rabab Mashayekhi <sup>3</sup>, Xiaoyi Zhao <sup>1</sup> and Henk Eskes <sup>4</sup>

<sup>1</sup> Air Quality Research Division, Environment and Climate Change Canada, Toronto, ON M3H 5T4, Canada; chris.mclinden@canada.ca (C.A.M.); mike.moran@canada.ca (M.D.M.); vitali.fioletov@canada.ca (V.F.); xiaoyi.zhao@canada.ca (X.Z.)

<sup>2</sup> Department of Physics and Engineering Physics, University of Saskatchewan, Saskatoon, SK S7N 5E2, Canada

<sup>3</sup> Canadian Meteorological Centre Operations Division, Environment and Climate Change Canada, Dorval, QC H9P 1J3, Canada; jacinthe.racine@canada.ca (J.R.); radenko.pavlovic@canada.ca (R.P.); rabab.mashayekhi@canada.ca (R.M.)

<sup>4</sup> Royal Netherlands Meteorological Institute (KNMI), 3731 GA De Bilt, The Netherlands; henk.eskes@knmi.nl

\* Correspondence: debora.griffin@canada.ca

Received: 16 October 2020; Accepted: 11 December 2020; Published: 16 December 2020



**Abstract:** A lockdown was implemented in Canada mid-March 2020 to limit the spread of COVID-19. In the wake of this lockdown, declines in nitrogen dioxide (NO<sub>2</sub>) were observed from the Tropospheric Monitoring Instrument (TROPOMI). A method is presented to quantify how much of this decrease is due to the lockdown itself as opposed to variability in meteorology and satellite sampling. The operational air quality forecast model, GEM-MACH (Global Environmental Multi-scale - Modelling Air quality and Chemistry), was used together with TROPOMI to determine expected NO<sub>2</sub> columns that represents what TROPOMI would have observed for a non-COVID scenario. Applying this methodology to southern Ontario, decreases in NO<sub>2</sub> emissions due to the lockdown were seen, with an average 40% (roughly 10 kt[NO<sub>2</sub>]/yr) in Toronto and Mississauga and even larger declines in the city center. Natural and satellite sampling variability accounted for as much as 20–30%, which demonstrates the importance of taking meteorology into account. A model run with reduced emissions (from 65 kt[NO<sub>2</sub>]/yr to 40 kt[NO<sub>2</sub>]/yr in the Greater Toronto Area) based on emission activity data during the lockdown period was found to be consistent with TROPOMI NO<sub>2</sub> columns.

**Keywords:** air pollution; TROPOMI; COVID; nitrogen oxides

## 1. Introduction

The outbreak of Coronavirus disease in late 2019 (COVID-19) reached Canada in early 2020, with the first Canadian COVID-related death reported in early March 2020 [1]. By mid-March, provinces were beginning to limit the size of gatherings and initiating an overall lockdown of their populations. In Ontario, the lockdown was announced on 16 March 2020. This greatly disrupted traffic patterns, with traffic density observed to decrease by roughly 50–60% by early April [2]. Travel restrictions also greatly curtailed air travel. These circumstances provided a unique and unprecedented natural experiment where emissions patterns were rapidly and drastically altered, especially in southern Ontario, home to the Greater Toronto Area (GTA), the most populous urban area in Canada [3]. The GTA consists of the City of Toronto and four surrounding regional municipalities (see Supplement Material Figure S1) and includes many limited-access highways and expressways, rail lines, and Toronto Pearson International Airport, Canada's busiest airport [4]. Its population in

2016 was over 6.4 million [3]. Ultimately, changing emissions in the GTA and the rest of southern Ontario associated with the pandemic allow for testing and refining of emissions from different sectors, most notably those from vehicle traffic.

One pollutant that is associated with combustion processes such as vehicle traffic is nitrogen dioxide ( $\text{NO}_x = \text{NO}_2 + \text{NO}$ ).  $\text{NO}_x$  has adverse effects on human and environmental health: it is a key ingredient in smog, as precursors to both ozone and particulate matter, and can contribute to acid deposition.  $\text{NO}_x$  concentrations strongly correlate with local emission sources due to its short lifetime of a few hours [5,6] and, because of the high and localized enhancements compared to background levels,  $\text{NO}_x$  is a good tracer of human activity near cities. For example, urban  $\text{NO}_x$  displays a strong weekly and diurnal cycle resulting from differences in traffic and manufacturing activity on weekends versus weekdays [7,8]. Observed  $\text{NO}_2$  is not merely a function of  $\text{NO}_x$  emissions; but is also a function of the local chemical environment and meteorology. For example, it is well known that  $\text{NO}_2$  impacts its own chemical lifetime [5]. Furthermore, meteorological parameters such as cloud cover, temperature, and wind speed and direction all have a strong effect on local  $\text{NO}_2$  enhancements [9–11]. Given this temporal and spatial variability in  $\text{NO}_2$ , precisely where and when observations are made is also very important. Taken together, one important challenge when interpreting changes in  $\text{NO}_2$  lies in disentangling potential changes in emissions from natural and sampling variability.

Satellite observations can help to identify  $\text{NO}_x$  emissions and their variation globally. Declines in  $\text{NO}_2$  emissions, following the lockdown, have previously been observed by satellite instruments in China, India, Europe and North America [12–15]. In this study, observations from the European Space Agency's Sentinel-5p Tropospheric Monitoring Instrument (TROPOMI), in conjunction with forecasts from Environment and Climate Change Canada's (ECCC) operational regional air quality forecast model GEM-MACH (Global Environmental Multi-scale - Modelling Air quality and CHEMistry) [16,17], are used to isolate the impact of the COVID associated lockdown on  $\text{NO}_2$  levels in southern Ontario, Canada. In this study, we show that combining satellite observations and model output, it is possible to determine the impact of meteorology and sampling variability on the observed  $\text{NO}_2$  column changes. The air quality model is further used to determine how possible lockdown-associated emission reductions impact the  $\text{NO}_2$  columns, and whether those match the observed changes.

## 2. Materials and Methods

In the context of satellite remote sensing, one method, and the most straightforward, to assess the impact of the COVID lockdown on  $\text{NO}_2$  is to directly compare the COVID period with a non-COVID period, perhaps using the same period from different years [13]. However, in order to completely isolate the COVID signal, this method assumes that among the two periods being compared, (i) baseline emissions do not differ, (ii) natural or seasonal variability in winds, sunlight, temperature, and other meteorological parameters are not important, (iii) differences in satellite sampling do not play any role, and (iv) any differences in the satellite retrieval algorithm are minimal. For many locations, including the Canadian domain studied here, differences in interannual  $\text{NO}_x$  emission changes should be small. However, meteorological variability can be important, and given that, sampling variability is also likely to lead to differences between the two periods. In the case of TROPOMI, different retrieval algorithms were used for spring 2019 vs. spring 2020 (v1.2 until April 2019 and thereafter v1.3, differences include the treatment of "negative" cloud fractions and the lower limit of the tropospheric air mass factor (AMF) relaxed influencing the quality flag [18]). While differences tend to be small, it is difficult at present to completely eliminate this as a possible source of difference.

With these confounding factors in mind, the method presented here is the one in which the ECCC's operational GEM-MACH air quality model forecasts are used to control for non-COVID factors such as sampling variability, meteorological variability, and other sources of variability. Furthermore, to limit potential differences in the retrieval algorithm between 2019 and 2020, the two periods considered are consecutive in 2020: a pre-COVID period and the COVID-lockdown period.

### 2.1. TROPOMI Observations

Observations of NO<sub>2</sub> from TROPOMI (2017-present [19]), an Earth-viewing spectrometer, are used here. TROPOMI has a resolution of  $3.5 \times 5.5 \text{ km}^2$  (since August 2019, before  $3.5 \times 7 \text{ km}^2$ ) at nadir and measures back-scattered ultraviolet/visible/solar-infrared sunlight from which NO<sub>2</sub> vertical column density (VCD), or the vertically-integrated NO<sub>2</sub> number density, can be derived. Details on the retrieval algorithm can be found elsewhere [20], but in short: a spectral fit is performed matching laboratory-measured NO<sub>2</sub> absorption cross-sections and other relevant parameters to these observed spectra which provide a determination of the NO<sub>2</sub> slant column densities (SCDs), or the number density integrated along the path of the sunlight through the atmosphere. In a second step, the stratospheric component of the SCD is determined using a chemical data assimilated system and subtracted [21]. Finally, the remaining tropospheric SCD is converted to a VCD using an AMF which quantifies the sensitivity of the satellite to a particular scene which depends on factors such as shape of the NO<sub>2</sub> profile, surface reflectivity, viewing geometry, and clouds. In this work, an alternative AMF is used which better accounts for the presence of snow and uses higher resolution NO<sub>2</sub> profile shapes to improve the effective spatial resolution [22,23]; see Supplement material for more information [24–33]. A radiative transfer model is used to calculate AMFs [34] which depend on the following factors: solar and viewing geometry, surface pressure, the presence and pressure of clouds, scene reflectivity and the vertical distribution of the NO<sub>2</sub> via  $\text{VCD} = \text{SCD} / \text{AMF}$ . Similar, as in the original TROPOMI AMF, the aerosols are corrected for implicitly [21]. Lastly, the TROPOMI data are filtered to use only the highest quality data ( $\text{qa\_value} > 0.75$  and the cloud cover of the pixels is at most 30%). The TROPOMI tropospheric NO<sub>2</sub> columns have been validated in a number of studies against ground-based, aircraft and other satellite observations [35–40]. The alternative AMFs have a smaller bias between ground-based and aircraft-borne observations over cities or near industry [23,41,42]. An evaluation of the TROPOMI NO<sub>2</sub> observations over the GTA in 2020 shows overall good agreement with ground-based remote-sensing PANDORA [43] measurements (see Figure S8).

### 2.2. GEM-MACH Air Quality Forecast Model

The Canadian operational air quality forecast model, GEM-MACH [16,17,44,45], is used in this work. GEM-MACH consists of an on-line chemical transport module that is embedded within ECCC's Global Environmental Multi-scale (GEM), weather forecast model, and is applied over a domain that covers most of North America. It includes emissions, chemistry, dispersion, and removal process representations for 41 gaseous and eight particle chemical species, and provides hourly concentrations between the surface and 0.1 Pa (on 80 hybrid vertical levels) with a  $10 \times 10 \text{ km}^2$  grid cell. The standard operational model run inputs hourly emissions fields that are prepared using the Sparse Matrix Operator Kernel Emissions (SMOKE) [46] that account for seasonal, weekly and daily variations. The performance of GEM-MACH has previously been evaluated against surface and remote-sensing measurements [16,44,47–51]. A performance evaluation of NO<sub>2</sub> forecasts for spring 2019 for Canada by the version of the air quality modelling system used in this study was carried out before it was implemented operationally in September 2019. As an indication of the quality of the pre-pandemic forecasts to be expected in this study, it was found that NO<sub>2</sub> forecasts for Canada for that period had a mean bias of 1.4 ppbv, a correlation coefficient of 0.57, and a root mean square error of 7.8 ppbv [48]. Additionally, an evaluation with PANDORA ground-based measurements was performed over the GTA for 2020, and showed overall good agreement with the model NO<sub>2</sub> VCDs (see Figure S9). The current version of the emissions files used by the operational model are based on a Canadian emissions inventory compiled for the 2013 base year and a 2017 projected U.S. inventory [48]. While using year-specific NO<sub>x</sub> emissions is ideal, suitable emission inventories are not available in a timely manner. Alternative non-operational runs were also performed for a limited time period between 15 March and 10 May 2020 with projected Canadian 2020 emissions and COVID-modified emissions for vehicle, aircraft, manufacturing, and residential sectors (see Section 3 for details). The Canadian 2020 anthropogenic emissions are based on projected national emission

inventory that was generated by ECCC for policy studies [52]. The projections include expected changes in population, economic activity and energy use over a five-year period, from 2015 to 2020.

GEM-MACH output is used in this study for two purposes. The first is to provide profile shapes which are used in the calculation of revised TROPOMI AMFs as discussed above in Section 2.1, following the method proposed by Palmer et al. [34] and McLinden et al. [22]. These alternative AMFs (not the operational TROPOMI AMFs) are used to convert TROPOMI SCDs into VCDs. Thus, it is possible to carry out the direct comparison between our TROPOMI NO<sub>2</sub> VCDs and those obtained from the GEM-MACH (further details can be found in the supplement material). The second is to determine the time evolution of NO<sub>2</sub> on standard “business as usual” (BAU) input emissions that do not account for COVID impacts, which can then be contrasted with that observed by TROPOMI. In both cases, NO<sub>2</sub> profiles are obtained from operational forecasts, are run at 10 km spatial resolution and are launched every 12 h (and every 24 h for the special runs).

In this study, we integrate the model NO<sub>2</sub> profiles to obtain VCD values. The operational GEM-MACH model currently does not include NO<sub>x</sub> sources in the free troposphere (such as lightning and aircraft at cruising altitude); as a consequence the model NO<sub>x</sub> concentrations are near zero above the boundary layer. We obtain a more realistic free tropospheric column from GEOS-Chem [53], a 3-D model of atmospheric chemistry model (monthly averages between 18–21 UTC, from 2 km to 12 km; 0.5 × 0.67° resolution, version v8-03-01; <http://www.geos-chem.org>), these partial columns are on the order of 10<sup>14</sup> molec/cm<sup>2</sup> and small compared to the partial columns in the boundary layer (see Figure S7), similar corrections have been applied in previous studies [22,23,49]. The model VCDs are then sampled (and filtered) in space and time at each TROPOMI pixel, and are filtered like the TROPOMI observations.

### 2.3. Determination of Expected NO<sub>2</sub>

GEM-MACH model output is used to estimate the impact of: (1) COVID measures on NO<sub>2</sub> levels, (2) changes from any other possible sources of variability, including seasonal, inter-annual, or even shorter-term meteorological variability, and (3) the TROPOMI sampling variability. GEM-MACH forecasts using standard emissions inventories for both the pre-lockdown and lockdown periods are sampled at each TROPOMI pixel and overpass time.

Comparing pre-lockdown and lockdown TROPOMI observations together with pre-lockdown and lockdown GEM-MACH predictions provides an estimate of the changes in NO<sub>x</sub> emissions purely due to the lockdown, as this method accounts for effects of meteorology, seasonality, and sampling variability. The expected TROPOMI VCDs,  $V_{T,e}$ , under a BAU scenario, are determined from the TROPOMI VCDs before the lockdown and are adjusted by the relative change seen in the model forecasts (GEM-MACH and free troposphere from GEOS-Chem) between the two time periods:

$$V_{T,e}(t_{covid}) = V_T(t_{pre}) \cdot \frac{V_{Model}(t_{covid})}{V_{Model}(t_{pre})}. \quad (1)$$

When averaging over time to produce spatially resolved maps, observations from 15 February to 15 March 2020 and 16 March to 8 May 2020 are used for the pre-lockdown and lockdown time periods, respectively. This end date is associated with some traffic rebound and increased emissions throughout May 2020 (see Section 3). When averaging over a larger area to produce a time series, 15-day running means are used (the satellite data need to be averaged over multiple days in order to obtain enough data over this area, approximately 50% of observations are filtered due to clouds). The expected columns for the 15-day running means are estimated as in Equation (1), where  $V_{T,e}(t_{covid})$  and  $V_{Model}(t_{covid})$  are the 15-day means for a specific day.

### 3. Results and Discussions

#### 3.1. Spatial Averaging over Southern Ontario

Figure 1 shows the TROPOMI and operational GEM-MACH NO<sub>2</sub> VCDs averaged over the pre-lockdown and lockdown periods. There is excellent agreement between TROPOMI, panel (a), and GEM-MACH, panel (d), across southern Ontario for the pre-lockdown period in terms of both spatial distribution and magnitudes which provides confidence that the NO<sub>x</sub> emissions inventory and the model itself can accurately represent the complex physics and photochemistry of the real world.

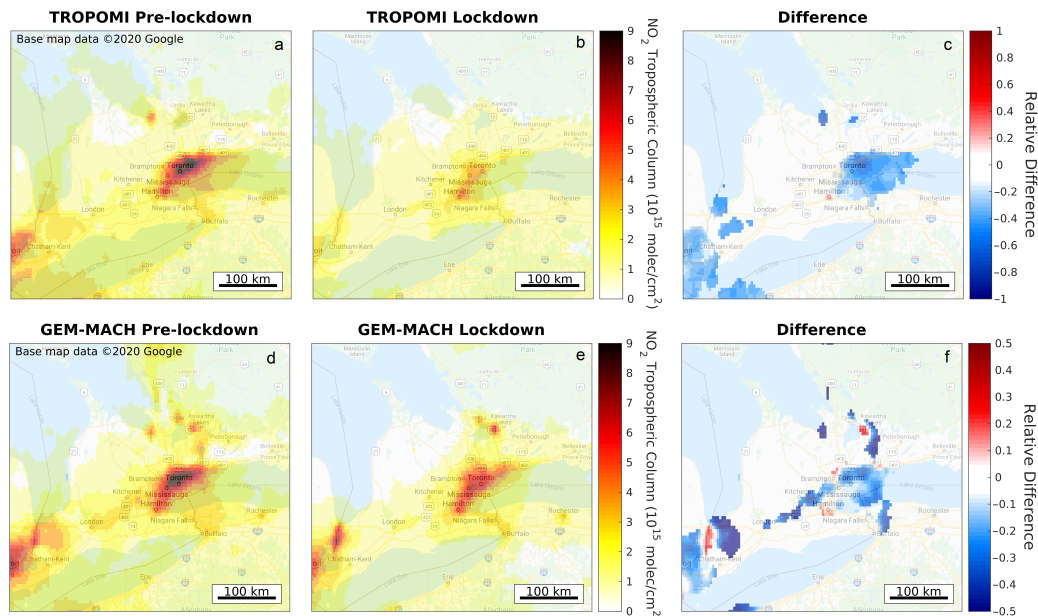


**Figure 1.** TROPOMI averaged VCDs over southern Ontario are shown for (a) a pre-lockdown (16 February–15 March 2020) and (b) a lockdown (16 March–8 May 2020) period. The relative differences ((lockdown-pre-lockdown)/pre-lockdown) are shown in panel (c) for areas that exceed  $3 \times 10^{15}$  molec/cm<sup>2</sup> in the pre-lockdown period. Panels (d–f) are the same but for the operational GEM-MACH model BAU NO<sub>2</sub> VCDs, sampled at the time and location of the TROPOMI pixels.

When comparing TROPOMI observations between the pre-lockdown and lockdown periods, panel (a)–(c), there is a large decrease in VCDs over the GTA, the Windsor-Detroit urban area (which straddles the Canada-U.S. border), and virtually the entire domain. Decreases in the urban areas can reach or exceed 50%, and in parts of the GTA the decline can even exceed 60%. However, there is also a decrease predicted by GEM-MACH, despite not accounting for COVID-related emissions reductions as shown in panels (d)–(f). This is due to a combination of a seasonal effect in which increased sunlight means a decrease in NO<sub>x</sub> lifetime and less NO<sub>x</sub> present as NO<sub>2</sub>, but also expected seasonal changes in emissions (see Supplement Material Figure S2). This effect is on the order of 25% over the GTA between the two time periods, and is especially large because it occurs during the change from cold season to warm season.

Even using several weeks of TROPOMI observations, meteorological and sampling variability can impact the average. Spring 2020 was colder than 2019 and particularly cloudy over southern Ontario, leading to fewer cloud-free overpasses on which to base an average. This can have an impact on the averages, since approximately 50% of TROPOMI data are removed due to cloud cover, so that the remaining cloud-free observations are more representative of fair weather conditions. To determine the impact of the sampling variability, GEM-MACH averages are determined using all days over the entire domain, versus only those sampled as TROPOMI ( $qa > 0.75$ ). For the average NO<sub>2</sub> between

16 March and 8 May 2020, sampling variability can lead to differences as large as 10% near cities (see Supplement material Figure S3).

As a test of the methodology to create expected TROPOMI columns for the COVID-19 period from the change in the model forecasts, the same procedure was applied to TROPOMI observations and operational GEM-MACH output from 2019. In this case, differences between expected and TROPOMI observations should be minimal, because no unusual emission reductions occurred in 2019. As can be seen in Figure 2d,e, differences are small, suggesting the method is generally reliable. Averaged over the GTA, differences are 0–2%.

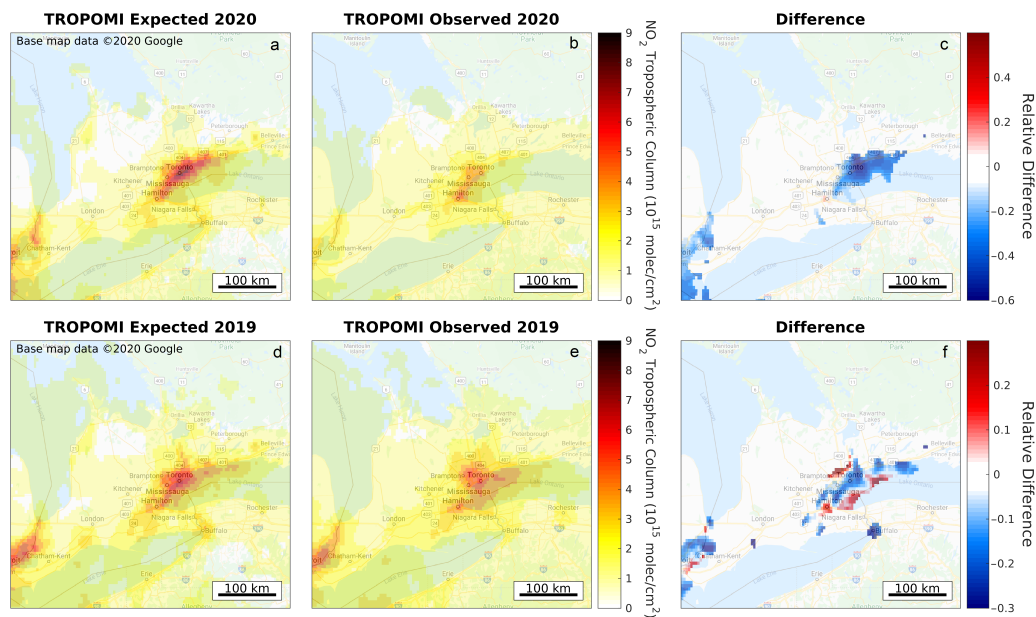


**Figure 2.** The figures show the expected and observed TROPOMI averaged NO<sub>2</sub> VCDs over southern Ontario for 2020 and 2019. Expected and observed TROPOMI average VCD fields for the lockdown period (16 March–8 May 2020) are shown in panels (a,b), respectively. The same is shown in panels (d,e), but for 16 March–8 May 2019. Relative differences ((observed-expected)/expected; for areas that exceed  $3 \times 10^{15}$  molec/cm<sup>2</sup>) between the TROPOMI observations and the expected columns are shown in panel (c,f) for 2020 and 2019, respectively. Note that panel (b) is the same as Figure 1b.

### 3.2. COVID-Scenario Model Run

To help evaluate the difference between expected and observed TROPOMI NO<sub>2</sub> columns, as shown in Figure 2, GEM-MACH is re-run using an alternative emissions scenario designed to represent COVID-19 emissions changes: (i) a 30% reduction in industrial NO<sub>x</sub> emissions, (ii) a 60% reduction for traffic NO<sub>x</sub> emissions, (iii) an 80% reduction in aircraft NO<sub>x</sub> emissions (landings and takeoffs), and (iv) a 20% increase of residential fuel NO<sub>x</sub> emissions due to people staying at home. Emissions of other air pollutants emitted by these source types (CO, VOC, NH<sub>3</sub>, SO<sub>2</sub>, PM<sub>2.5</sub>, PM<sub>10</sub>) are also changed by these same percentages. The change of emissions is based on the following: (i) similar emission scenarios from Europe [11], (ii) an estimate of daily driving activities which showed a reduction of 50–65% decrease [2], (iii) the reduction of airline flights which were 79% lower in April 2020 compared to April 2019 [54], and (iv) Google mobility Reports [55] showed an increase spent in residential spaces and thus an increase of 20% is applied to residential emissions. Over the entire GTA, average emissions decline from 65 kt[NO<sub>2</sub>]/yr pre-lockdown to 40 kt[NO<sub>2</sub>]/yr lockdown (around noon; see Figures S3, S5, S6, and Table S2). Note that only Canadian emissions are adjusted in this way due to the challenge of representing the complicated mixture of city-, county-, and state-level responses to COVID-19 in the U.S., but given the short atmospheric lifetime of NO<sub>x</sub> this is unlikely to make a big difference to NO<sub>2</sub> levels except close to the international border (further details can be found in the supplement on the impact of trans-border NO<sub>2</sub> transport, Figure S10).

The results of this emissions scenario run are shown and compared to TROPOMI observations in Figure 3 (for 1 April to 8 May 2020). Good agreement is evident over much of southern Ontario. The TROPOMI observations are approximately 20–30% higher than the model output in Hamilton (an industrial city), where industry emissions might be underestimated, and parts of Mississauga, where airport or vehicle traffic emissions might be underestimated in the model run.

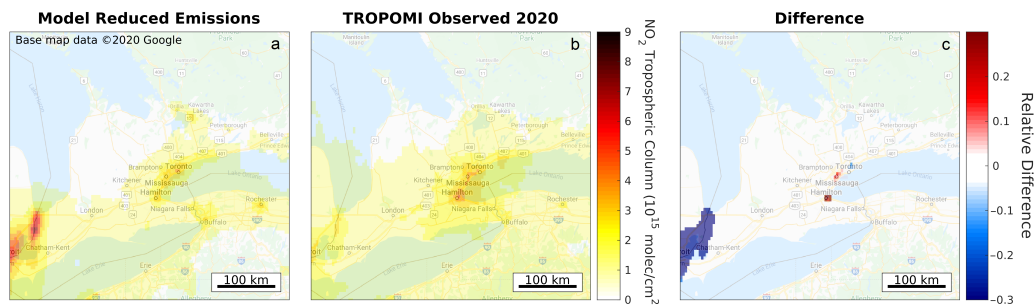


**Figure 3.** Model NO<sub>2</sub> VCDs from the reduced emissions scenario (a) and observed TROPOMI NO<sub>2</sub> VCDs (b) over southern Ontario averaged over the period 1 April – 8 May 2020. The relative differences ((observations-model)/model) are shown in panel (c) for areas that exceed  $3 \times 10^{15}$  molec/cm<sup>2</sup>. Note that emissions have only been reduced in Canada; thus, large differences can be seen for the US cities near the border, especially Detroit.

### 3.3. Temporal Changes over Toronto

An alternative method of considering these various data sources is to average spatially and look at temporal changes. Figure 4 shows a time series of 15-day running average NO<sub>2</sub> over the Toronto and Mississauga area (part of the GTA with the highest emissions and population density, this area also includes Toronto Pearson Airport; see Supplement Material Figure S1). TROPOMI observations show a decline after the lockdown was announced (Figure 4a), the expected columns agree well with the TROPOMI observations during the pre-lockdown period, but, differences emerge after the lockdown begins as emissions are reduced, but the model assumes BAU emissions. The alternate model run with reduced emissions (Figure 4b) represents the decline observed by TROPOMI quite well and over the same time period, both the TROPOMI observations and the model predict a drop of roughly 40% over the GTA core (using data from 16 March to 8 May 2020) as a result of the lockdown. When the 2019 and 2020 satellite data are compared directly, however, the drop is only about half as much (20%), as the meteorology and sampling variability of the satellite are largely different in that area between 2019 and 2020. Note that the satellite data indicate that the peak of the emissions decline in Toronto and Mississauga occurred in mid-April. Throughout May 2020, the satellite measurements suggest that the NO<sub>x</sub> emissions began to increase again gradually (Figure 4a), though they are still lower than BAU emissions. Ontario entered Phase 1 of its re-opening on 19 May 2020, when certain restrictions were lifted.

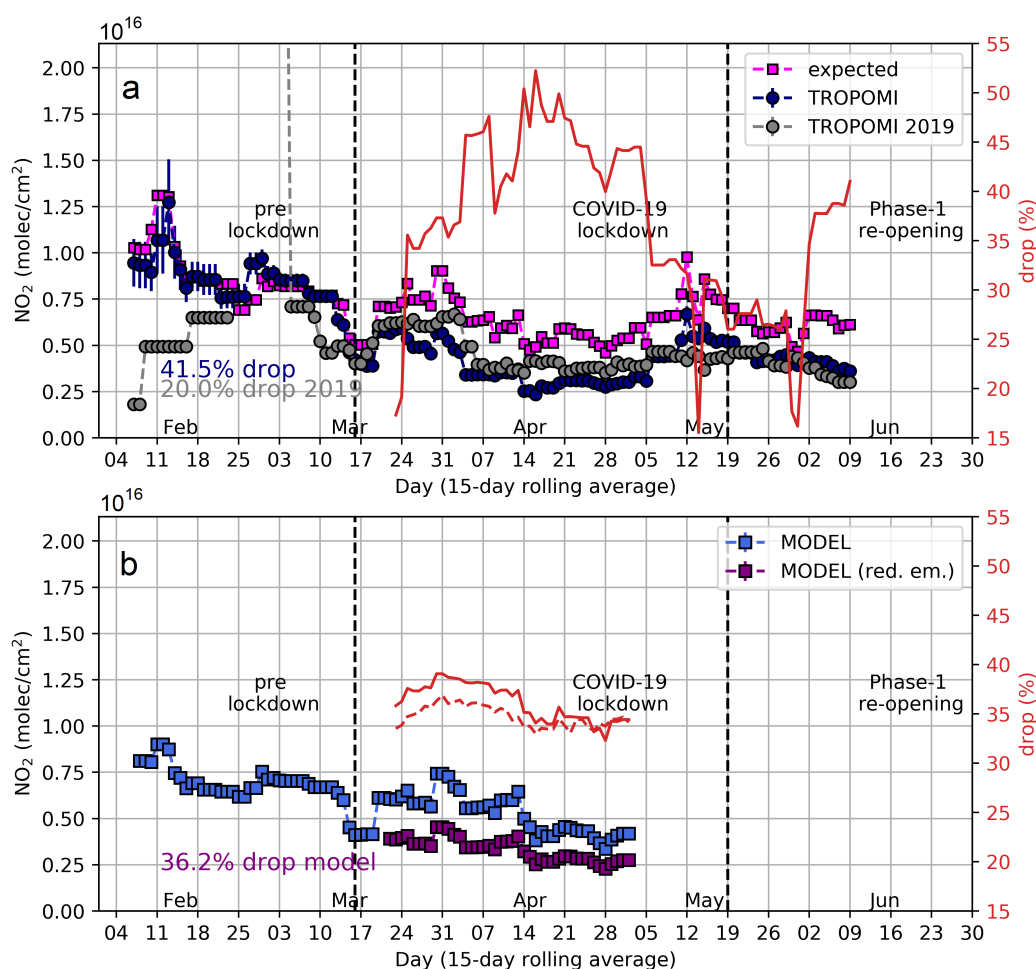


**Figure 4.** Timeseries of 15-day running mean of  $\text{NO}_2$  VCDs over Toronto and Mississauga for 7 February to 9 June 2020, panel (a) shows the TROPOMI observations (navy), the expected columns (magenta). The timeseries of 2019 TROPOMI observations (grey) for the same period is shown as a reference. The red line indicates the percentage emission reductions based on the difference between the TROPOMI observations and expected columns. Panel (b) shows  $\text{NO}_2$  columns from the model predictions sampled like TROPOMI assuming a BAU scenario with 2020 updated emissions (blue) and a 2020 COVID reduced emissions scenario (purple). The percentage decrease in model predicted VCDs (red line) is estimated from the difference between the two model runs, the red dashed line shows the drop for perfect sampling. Average emission reductions are highlighted using observations between 16 March to 8 May 2020. Approximately 200 observations are averaged for the 15-day mean, the resulting standard errors are plotted, however, the standard error is seen to be small and on the order of  $10^{13}$ – $10^{14}$  molec/cm<sup>2</sup>.

#### 4. Conclusions

We present a method to disentangle the effects of meteorology and sampling variability on the observed  $\text{NO}_2$  changes, from the lockdown-related changes in  $\text{NO}_x$  emissions. During the period from 16 March to 8 May 2020,  $\text{NO}_2$  columns in the center of the GTA decreased by nearly 60% compared to the previous month. About 25% of this decrease is associated with meteorological and seasonal changes independent of the COVID-19 pandemic. Even the TROPOMI sampling variability itself can impact the magnitude of the observed  $\text{NO}_2$  columns over the course of one or two months averaging ( $\sim 10\%$ ). From the TROPOMI observations and GEM-MACH air quality model results, we estimate that due to the lockdown the  $\text{NO}_2$  columns in Toronto and Mississauga declined by over 40%. These changes vary spatially, and in certain locations columns declined by over 50%. Applying the same method to

2019 observations leads to a 0–2% decline over the GTA, which is expected as there were no emission declines in spring 2019, which gives confidence that the method is robust.

A special model run with reduced NO<sub>x</sub> emissions of vehicle traffic, aircraft, and industry based on lockdown activity data [2,54,55] compares well with the TROPOMI observations during the lockdown and returned similar NO<sub>2</sub> declines in the GTA. Although, spatial patterns over cities are somewhat visible, it is hard to disentangle the emission reductions by sector with our methodology. Nevertheless, emission changes of (i) a 30% reduction in industry, (ii) a 60% reduction for traffic, (iii) an 80% reduction in aircraft landings and takeoffs, and (iv) a 20% increase in residential fuel combustion, represent the TROPOMI NO<sub>2</sub> observations well, at least in southern Ontario. In the GTA, NO<sub>x</sub> emissions of 40 kt[NO<sub>2</sub>]/yr represent the observations well, this is a drop of over 37% compared to a BAU scenario. The drop in the input emissions is almost identical to the drop determined from the model NO<sub>2</sub> VCDs (36%) over the same area which further indicates that the method presented works well.

This study highlights the importance of considering meteorological and sampling variability when estimating emission reductions. One needs to be cautious when simply comparing two months, since the effects of meteorological and sampling variability are not negligible when only a short series of data is averaged. We show that spring 2019 and 2020 were, with regards to the meteorology, very different years and simply looking at the difference results in about half the NO<sub>x</sub> emission decline as compared to considering the meteorology. Further, the emission decline may vary strongly spatially, especially in cities. This can make it difficult to compare different studies unless the exact same areas are considered. The unique lockdown period associated with the 2020 COVID-19 pandemic can further be used to check and refine our existing emissions inventories for NO<sub>x</sub> and other pollutants by looking at spatial and temporal distributions of available satellite and surface measurements for a number of different urban areas.

**Supplementary Materials:** The following are available online at <http://www.mdpi.com/2072-4292/12/24/4112/s1>, Figure S1: Boundaries of the Greater Toronto Area, Figure S2: Operational forecast model's seasonal emission changes, Figure S3: Impact of the sampling on the averaged TROPOMI columns, Figure S4: Model input NO<sub>x</sub> emissions, Figure S5: Model input emissions in Toronto and Mississauga, Figure S6: Correlation between TROPOMI observations and model VCDs, Figure S7: Correlation between TROPOMI observations and model VCDs with and without free-tropospheric column, Figure S8: Comparison between TROPOMI and ground-based PANDORA NO<sub>2</sub> measurements, Figure S9: Comparison between model and ground-based PANDORA NO<sub>2</sub> measurements, Figure S10: Impact of US NO<sub>2</sub> emission changes on the GTA NO<sub>2</sub> concentrations, Table S1: Parameters and their reference points in the AMF look-up table, Table S2: Approximate average emissions used for the model runs in the GTA, Table S3: The statistics from the model and TROPOMI comparison.

**Author Contributions:** Conceptualization, D.G., C.A.M., M.D.M., and V.F.; methodology, D.G., C.A.M., M.D.M., V.F., J.R., R.M. and R.P.; software, D.G., and J.R.; validation, C.A.M., M.D.M., V.F., and X.Z.; formal analysis, D.G., J.R., and R.M.; investigation, D.G. and C.A.M.; resources, R.P., and H.E.; data curation, J.R., R.M., and H.E.; writing—original draft preparation, D.G. and C.A.M.; writing—review and editing, all authors; visualization, D.G., C.A.M., and X.Z.; supervision, C.A.M. and R.P. All authors have read and agreed to the published version of the manuscript.

**Funding:** This work contains modified Copernicus Sentinel data. The Sentinel 5 Precursor TROPOMI Level 2 product is developed with funding from the Netherlands Space Office (NSO) and processed with funding from the European Space. TROPOMI data can be downloaded from <https://s5phub.copernicus.eu> (last access: 6 June 2020).

**Acknowledgments:** We would like to thank you MSC-REQA employees involved in emission adjustment and modelling: Mourad Sassi, Annie Duhamel and Jessica Miville.

**Conflicts of Interest:** The authors declare no conflict of interest.

## References

1. Statistics Canada. Provisional Death Counts and Excess Mortality, January to April 2019 and January to April 2020. Available online: <https://www150.statcan.gc.ca/n1/daily-quotidien/200619/dq200619b-eng.htm> (accessed on 29 September 2020).
2. Apple. COVID-19 Mobility Trends Reports. 2020. Available online: <https://covid19.apple.com/mobility> (accessed on 29 September 2020).

3. Statistics Canada. Population and Dwelling Count Highlight Tables, 2016 Census. 2019. Available online: <https://www12.statcan.gc.ca/census-recensement/2016/dp-pd/hlt-fst/pd-pl/Table.cfm?Lang=Eng&T=801&SR=1&S=3&O=D&RPP=25&PR=0&CMA=0#tPopDwell> (accessed on 29 September 2020).
4. Statistics Canada. Table: 23-10-0253-01, Air Passenger Traffic at Canadian Airports, Annual. 2020. Available online: <https://doi.org/10.25318/2310025301-eng> (accessed on 29 September 2020).
5. Valin, L.C.; Russell, A.R.; Cohen, R.C. Variations of OH radical in an urban plume inferred from NO<sub>2</sub> column measurements. *Geophys. Res. Lett.* **2013**, *40*, 1856–1860. [[CrossRef](#)]
6. Beirle, S.; Boersma, K.F.; Platt, U.; Lawrence, M.G.; Wagner, T. Megacity Emissions and Lifetimes of Nitrogen Oxides Probed from Space. *Science* **2011**, *333*, 1737–1739. [[PubMed](#)]
7. Beirle, S.; Platt, U.; Wenig, M.; Wagner, T. Weekly cycle of NO<sub>2</sub> by GOME measurements: A signature of anthropogenic sources. *Atmos. Chem. Phys.* **2003**, *3*, 2225–2232. [[CrossRef](#)]
8. De Foy, B.; Lu, Z.; Streets, D.G. Satellite NO<sub>2</sub> retrievals suggest China has exceeded its NO<sub>x</sub> reduction goals from the twelfth Five-Year Plan. *Sci. Rep.* **2016**, *6*. [[CrossRef](#)] [[PubMed](#)]
9. Goldberg, D.L.; Anenberg, S.C.; Griffin, D.; McLinden, C.A.; Lu, Z.; Streets, D.G. Disentangling the Impact of the COVID-19 Lockdowns on Urban NO<sub>2</sub> From Natural Variability. *Geophys. Res. Lett.* **2020**, *47*, e2020GL089269, [[CrossRef](#)]
10. Wang, P.; Chen, K.; Zhu, S.; Wang, P.; Zhang, H. Severe air pollution events not avoided by reduced anthropogenic activities during COVID-19 outbreak. *Resour. Conserv. Recycl.* **2020**, *158*, 104814. [[CrossRef](#)]
11. Menuet, L.; Bessagnet, B.; Siour, G.; Mailler, S.; Pennel, R.; Cholakian, A. Impact of lockdown measures to combat Covid-19 on air quality over western Europe. *Sci. Total Environ.* **2020**, *741*, 140426. [[CrossRef](#)]
12. Zhang, R.; Zhang, Y.; Lin, H.; Feng, X.; Fu, T.M.; Wang, Y. NO<sub>x</sub> Emission Reduction and Recovery during COVID-19 in East China. *Atmosphere* **2020**, *11*, 433. [[CrossRef](#)]
13. Bauwens, M.; Compennolle, S.; Stavrakou, T.; Müller, J.F.; van Gent, J.; Eskes, H.; Levelt, P.F.; van der A, R.; Veefkind, J.P.; Vlietinck, J.; et al. Impact of coronavirus outbreak on NO<sub>2</sub> pollution assessed using TROPOMI and OMI observations. *Geophys. Res. Lett.* **2020**, e2020GL087978, [[CrossRef](#)]
14. Shi, X.; Brasseur, G.P. The Response in Air Quality to the Reduction of Chinese Economic Activities during the COVID-19 Outbreak. *Geophys. Res. Lett.* **2020**, e2020GL088070, [[CrossRef](#)]
15. Adams, M.D. Air pollution in Ontario, Canada during the COVID-19 State of Emergency. *Sci. Total Environ.* **2020**, *742*, 140516. [[CrossRef](#)] [[PubMed](#)]
16. Moran, M.D.; Ménard, S.; Talbot, D.; Huang, P.; Makar, P.A.; Gong, W.; Landry, H.; Gravel, S.; Gong, S.; Crevier, L.P.; et al. Particulate-matter forecasting with GEM-MACH15, a new Canadian air-quality forecast model. In *Air Pollution Modelling and Its Application XX*; Springer: Dordrecht, The Netherlands, 2010.
17. Pendlebury, D.; Gravel, S.; Moran, M.D.; Lupu, A. Impact of chemical lateral boundary conditions in a regional air quality forecast model on surface ozone predictions during stratospheric intrusions. *Atmos. Environ.* **2018**, *174*, 148–170. [[CrossRef](#)]
18. Copernicus. Data Products: Nitrogen Dioxide. 2020. Available online: <http://www.tropomi.eu/data-products/nitrogen-dioxide> (accessed on 29 September 2020).
19. Veefkind, J.; Aben, I.; McMullan, K.; Forster, H.; de Vries, J.; Otter, G.; Claas, J.; Eskes, H.; de Haan, J.; Kleipool, Q.; et al. TROPOMI on the ESA Sentinel-5 Precursor: A GMES mission for global observations of the atmospheric composition for climate, air quality and ozone layer applications. *Remote Sens. Environ.* **2012**, *120*, 70–83. [[CrossRef](#)]
20. van Geffen, J.; Boersma, K.F.; Eskes, H.; Sneep, M.; ter Linden, M.; Zara, M.; Veefkind, J.P. S5P/TROPOMI NO<sub>2</sub> slant column retrieval: Method, stability, uncertainties, and comparisons against OMI. *Atmos. Meas. Tech. Dis.* **2019**, *2019*, 1–33. [[CrossRef](#)]
21. van Geffen, J.H.G.M.; Eskes, H.J.; Boersma, K.F.; Maasackers, J.D.; Veefkind, J.P. TROPOMI ATBD of the Total and Tropospheric NO<sub>2</sub> Data Products; Issue 1.2.0 ed., 2018. S5P-KNMI-L2-0005-RP. Available online: <https://sentinel.esa.int/documents/247904/2476257/Sentinel-5P-TROPOMI-ATBD-NO2-data-products> (accessed on 28 September 2020).

22. McLinden, C.A.; Fioletov, V.; Boersma, K.F.; Kharol, S.K.; Krotkov, N.; Lamsal, L.; Makar, P.A.; Martin, R.V.; Veefkind, J.P.; Yang, K. Improved satellite retrievals of NO<sub>2</sub> and SO<sub>2</sub> over the Canadian oil sands and comparisons with surface measurements. *Atmos. Chem. Phys.* **2014**, *14*, 3637–3656. [[CrossRef](#)]
23. Griffin, D.; Zhao, X.; McLinden, C.A.; Boersma, F.; Bourassa, A.; Dammers, E.; Degenstein, D.; Eskes, H.; Fehr, L.; Fioletov, V.; et al. High-Resolution Mapping of Nitrogen Dioxide With TROPOMI: First Results and Validation Over the Canadian Oil Sands. *Geophys. Res. Lett.* **2019**, *46*, 1049–1060. [[CrossRef](#)]
24. Côté, J.; Gravel, S.; Méthot, A.; Patoine, A.; Roch, M.; Staniforth, A. The Operational CMC–MRB Global Environmental Multiscale (GEM) Model. Part I: Design Considerations and Formulation. *Mon. Weather Rev.* **1998**, *126*, 1373–1395. [[CrossRef](#)]
25. Girard, C.; Plante, A.; Desgagné, M.; McTaggart-Cowan, R.; Côté, J.; Charron, M.; Gravel, S.; Lee, V.; Patoine, A.; Qaddouri, A.; et al. Staggered Vertical Discretization of the Canadian Environmental Multiscale (GEM) Model Using a Coordinate of the Log-Hydrostatic-Pressure Type. *Mon. Weather Rev.* **2014**, *142*, 1183–1196. [[CrossRef](#)]
26. Houyoux, M.R.; Vukovich, J.M.; Coats, C.J., Jr.; Wheeler, N.J.M.; Kasibhatla, P.S. Emission inventory development and processing for the Seasonal Model for Regional Air Quality (SMRAQ) project. *J. Geophys. Res. Atmos.* **2000**, *105*, 9079–9090. [[CrossRef](#)]
27. Schaaf, C.B.; Gao, F.; Strahler, A.H.; Lucht, W.; Li, X.; Tsang, T.; Strugnell, N.C.; Zhang, X.; Jin, Y.; Muller, J.P.; et al. First operational BRDF, albedo nadir reflectance products from MODIS. *Remote Sens. Environ.* **2002**, *83*, 135–148. [[CrossRef](#)]
28. Makar, P.A.; Gong, W.; Milbrandt, J.; Hogrefe, C.; Zhang, Y.; Curci, G.; Žabkar, R.; Im, U.; Balzarini, A.; Baró, R.; et al. Feedbacks between air pollution and weather, Part 1: Effects on weather. *Atmos. Environ.* **2015**, *115*, 442–469. [[CrossRef](#)]
29. Makar, P.A.; Gong, W.; Hogrefe, C.; Zhang, Y.; Curci, G.; Žabkar, R.; Milbrandt, J.; Im, U.; Balzarini, A.; Baró, R.; et al. Feedbacks between air pollution and weather, part 2: Effects on chemistry. *Atmos. Environ.* **2015**, *115*, 499–526. [[CrossRef](#)]
30. Gong, W.; Makar, P.; Zhang, J.; Milbrandt, J.; Gravel, S.; Hayden, K.; Macdonald, A.; Leaitch, W. Modelling aerosol–cloud–meteorology interaction: A case study with a fully coupled air quality model (GEM-MACH). *Atmos. Environ.* **2015**, *115*, 695–715. [[CrossRef](#)]
31. Gong, W.; Beagley, S.R.; Cousineau, S.; Sassi, M.; Munoz-Alpizar, R.; Ménard, S.; Racine, J.; Zhang, J.; Chen, J.; Morrison, H.; et al. Assessing the impact of shipping emissions on air pollution in the Canadian Arctic and northern regions: Current and future modelled scenarios. *Atmos. Chem. Phys.* **2018**, *18*, 16653–16687. [[CrossRef](#)]
32. Akingunola, A.; Makar, P.A.; Zhang, J.; Darlington, A.; Li, S.M.; Gordon, M.; Moran, M.D.; Zheng, Q. A chemical transport model study of plume-rise and particle size distribution for the Athabasca oil sands. *Atmos. Chem. Phys.* **2018**, *18*, 8667–8688. [[CrossRef](#)]
33. Cooper, M.J.; Martin, R.V.; Lyapustin, A.I.; McLinden, C.A. Assessing snow extent data sets over North America to inform and improve trace gas retrievals from solar backscatter. *Atmos. Meas. Tech.* **2018**, *11*, 2983–2994. [[CrossRef](#)]
34. Palmer, P.I.; Jacob, D.J.; Chance, K.; Martin, R.V.; Spurr, R.J.D.; Kurosu, T.P.; Bey, I.; Yantosca, R.; Fiore, A.; Li, Q. Air mass factor formulation for spectroscopic measurements from satellites: Application to formaldehyde retrievals from the Global Ozone Monitoring Experiment. *J. Geophys. Res. Atmos.* **2001**, *106*, 14539–14550. [[CrossRef](#)]
35. Verhoelst, T.; Compernelle, S.; Pinardi, G.; Lambert, J.C.; Eskes, H.J.; Eichmann, K.U.; Fjæraa, A.M.; Granville, J.; Niemeijer, S.; Cede, A.; et al. Ground-based validation of the Copernicus Sentinel-5p TROPOMI NO<sub>2</sub> measurements with the NDACC ZSL-DOAS, MAX-DOAS and Pandonia global networks. *Atmos. Meas. Tech. Dis.* **2020**, *2020*, 1–40. [[CrossRef](#)]
36. Van Geffen, J.; Boersma, K.F.; Eskes, H.; Sneep, M.; ter Linden, M.; Zara, M.; Veefkind, J.P. S5P TROPOMI NO<sub>2</sub> slant column retrieval: Method, stability, uncertainties and comparisons with OMI. *Atmos. Meas. Tech.* **2020**, *13*, 1315–1335. [[CrossRef](#)]
37. Wang, P.; Piters, A.; van Geffen, J.; Tuinder, O.; Stammes, P.; Kinne, S. Shipborne MAX-DOAS measurements for validation of TROPOMI NO<sub>2</sub> products. *Atmos. Meas. Tech.* **2020**, *13*, 1413–1426. [[CrossRef](#)]

38. Dimitropoulou, E.; Hendrick, F.; Pinardi, G.; Friedrich, M.M.; Merlaud, A.; Tack, F.; De Longueville, H.; Fayt, C.; Hermans, C.; Laffineur, Q.; et al. Validation of TROPOMI tropospheric NO<sub>2</sub> columns using dual-scan MAX-DOAS measurements in Uccle, Brussels. *Atmos. Meas. Tech. Dis.* **2020**, *2020*, 1–50. [[CrossRef](#)]
39. Ialongo, I.; Virta, H.; Eskes, H.; Hovila, J.; Douros, J. Comparison of TROPOMI/Sentinel-5 Precursor NO<sub>2</sub> observations with ground-based measurements in Helsinki. *Atmos. Meas. Tech.* **2020**, *13*, 205–218. [[CrossRef](#)]
40. Tack, F.; Merlaud, A.; Iordache, M.D.; Pinardi, G.; Dimitropoulou, E.; Eskes, H.; Bomans, B.; Veeffkind, P.; Van Roozendaal, M. Assessment of the TROPOMI tropospheric NO<sub>2</sub> product based on airborne APEX observations. *Atmos. Meas. Tech. Dis.* **2020**, *2020*, 1–55. [[CrossRef](#)]
41. Zhao, X.; Griffin, D.; Fioletov, V.; McLinden, C.; Cede, A.; Tiefengraber, M.; Müller, M.; Bogner, K.; Strong, K.; Boersma, F.; et al. Assessment of the quality of TROPOMI high-spatial-resolution NO<sub>2</sub> data products in the Greater Toronto Area. *Atmos. Meas. Tech.* **2020**, *13*, 2131–2159. [[CrossRef](#)]
42. Goldberg, D.L.; Lu, Z.; Streets, D.G.; de Foy, B.; Griffin, D.; McLinden, C.A.; Lamsal, L.N.; Krotkov, N.A.; Eskes, H. Enhanced Capabilities of TROPOMI NO<sub>2</sub>: Estimating NO<sub>x</sub> from North American Cities and Power Plants. *Environ. Sci. Technol.* **2019**, *53*, 12594–12601, [[CrossRef](#)] [[PubMed](#)]
43. Herman, J.; Cede, A.; Spinei, E.; Mount, G.; Tzortziou, M.; Abuhassan, N. NO<sub>2</sub> column amounts from ground-based Pandora and MFDOAS spectrometers using the direct-sun DOAS technique: Intercomparisons and application to OMI validation. *J. Geophys. Res. Atmos.* **2009**, *114*. [[CrossRef](#)]
44. Pavlovic, R.; Chen, J.; Anderson, K.; Moran, M.D.; Beaulieu, P.A.; Davignon, D.; Cousineau, S. The FireWork air quality forecast system with near-real-time biomass burning emissions: Recent developments and evaluation of performance for the 2015 North American wildfire season. *J. Air Waste Manag. Assoc.* **2016**, *66*, 819–841. [[CrossRef](#)]
45. Makar, P.A.; Staebler, R.M.; Akingunola, A.; Zhang, J.; McLinden, C.; Kharol, S.K.; Pabla, B.; Cheung, P.; Zheng, Q. The effects of forest canopy shading and turbulence on boundary layer ozone. *Nat. Commun.* **2017**, *8*. [[CrossRef](#)]
46. Coats, C.J. High-performance algorithms in the sparse matrix operator kernel emissions (SMOKE) modeling system. In Proceedings of the Ninth AMS Joint Conference on Applications of Air Pollution Meteorology with AWMA, Atlanta, GA, USA, 28 January–2 February 1996.
47. Robichaud, A.; Ménard, R.; Zaitseva, Y.; Anselmo, D. Multi-pollutant surface objective analyses and mapping of air quality health index over North America. *Air Qual. Atmos. Health* **2016**, *9*, 743–759. [[CrossRef](#)]
48. Moran, M.D.; Ménard, S. Regional Air Quality Deterministic Prediction System (RAQDPS): Update from Version 020.2 to Version 021; Canadian Centre for Meteorological and Environmental Prediction: Montreal, CA, 2019. Technical Note, p. 49. Available online: [http://collaboration.cmc.ec.gc.ca/cmc/cmci/product\\_guide/docs/tech\\_notes/technote\\_raqdps-021\\_20190703\\_e.pdf](http://collaboration.cmc.ec.gc.ca/cmc/cmci/product_guide/docs/tech_notes/technote_raqdps-021_20190703_e.pdf) (accessed on 23 June 2020).
49. Zhao, X.; Griffin, D.; Fioletov, V.; McLinden, C.; Davies, J.; Ogyu, A.; Lee, S.C.; Lupu, A.; Moran, M.D.; Cede, A.; et al. Retrieval of total column and surface NO<sub>2</sub> from Pandora zenith-sky measurements. *Atmos. Chem. Phys.* **2019**, *19*, 10619–10642. [[CrossRef](#)]
50. Stroud, C.A.; Zaganescu, C.; Chen, J.; McLinden, C.A.; Zhang, J.; Wang, D. Toxic volatile organic air pollutants across Canada: Multi-year concentration trends, regional air quality modelling and source apportionment. *J. Atmos. Chem.* **2016**, *73*. [[CrossRef](#)]
51. Stroud, C.A.; Ren, S.; Zang, Z.; Akingunola, A.; Makar, P.; Munoz-Alpizar, R.; Leroyer, S.; Belair, S.; Sills, D.; Brook, J. Chemical analysis of surface-level ozone exceedances during the 2015 Pan American Games. *Atmosphere* **2020**, *11*, 37. [[CrossRef](#)]
52. APEI. Air Pollutant Emissions Inventory: Overview, Government of Canada. 2020. Available online: <https://www.canada.ca/en/environment-climate-change/services/pollutants/air-emissions-inventory-overview.html> (accessed on 28 September 2020).
53. Bey, I.; Jacob, D.J.; Yantosca, R.M.; Logan, J.A.; Field, B.D.; Fiore, A.M.; Li, Q.; Liu, H.Y.; Mickley, L.J.; Schultz, M.G. Global modeling of tropospheric chemistry with assimilated meteorology: Model description and evaluation. *J. Geophys. Res. Atmos.* **2001**, *106*, 23073–23095. [[CrossRef](#)]
54. Statistics Canada. Table 23-10-0003-01. Aircraft Movements, by Civil and Military Movements, Airports with NAV CANADA Towers, Monthly. 2020. Available online: <https://doi.org/10.25318/2310000301-eng> (accessed on 29 September 2020).

55. Google. COVID-19 Community Mobility Reports. 2020. Available online: <https://www.google.com/covid19/mobility/> (accessed on 29 September 2020).

**Publisher’s Note:** MDPI stays neutral with regard to jurisdictional claims in published maps and institutional affiliations.



© 2020 by the authors. Licensee MDPI, Basel, Switzerland. This article is an open access article distributed under the terms and conditions of the Creative Commons Attribution (CC BY) license (<http://creativecommons.org/licenses/by/4.0/>).